

On-Line Stability Margin and Attitude Estimation for Dynamic Articulating Mobile Robots

Antonio Diaz-Calderon¹ and Alonzo Kelly²

¹ Jet Propulsion Laboratory
California Institute of Technology
adiaz@jpl.nasa.gov
<http://telerobotics.jpl.nasa.gov/adiaz>

² The Robotics Institute
Carnegie Mellon University
alonzo@ri.cmu.edu
<http://www.frc.ri.cmu.edu/alonzo>

Abstract. Stability is an important concern for vehicles which move heavy loads, accelerate or brake aggressively, turn at speed, or operate on sloped terrain. In many cases, vehicles face more than one of these challenges simultaneously. Some are obliged to execute these maneuvers when their high centers of gravity leave them particularly vulnerable to tipover or rollover. A methodology is presented to estimate proximity to tipover for autonomous field robots which must be productive, effective, and self reliant under such challenging circumstances. While the physical principles governing the computation of stability margin have been known for some time, the realization of these principles in practice raises issues which are at once similar to those of attitude estimation while contrasting heavily with inertial guidance. The problem of stability margin estimation is posed in the fairly general case of accelerated articulating motion over rough terrain. Compatibility with and distinctions from attitude estimation lead to a proposed integrated solution to both problems based on the fusion of inertial, articulation, and terrain relative velocity sensing in an optimal estimation framework. An implementation of a device targeted to an industrial lift truck is presented.

1 Introduction

The term instability event will be used to refer to situations where a vehicle loses contact with the ground due to the application of unbalanced moments. If the associated rotation occurs around the longitudinal axis, the event will be called a rollover whereas motion around a lateral axis will be called a tipover. This article addresses the problem of detecting proximity to an instability event for articulating mobile robots subject to large inertial accelerations. When articulating, the location of the center of mass (denoted *cg* hereafter) of the system is not fixed and the problem requires additional attention to track the *cg* motion. We present the principles behind measuring and transforming the desired quantities in several cases of increasing complexity. Then, a Kalman filter instantiation is presented which computes the stability margin for a specific implementation. The filter is configured to evaluate alternative sensing and to operate as an attitude reference while estimating stability margin.

1.1 Motivation

The topic of wheeled mobile robot dynamic stability is presently somewhat rare in the literature relative to the more mainstream topics of environmental perception, cognition, and localization. This work is motivated by the observation that many potential applications will require such vehicles to operate on slopes and/or at high speeds for potentially extended periods of time. This is clear because contemporary mining, forestry, agriculture, and military vehicles do so today. Even for vehicles in transit from one place to another, it is often faster to go over a ridge than around it. For vehicles operating on slopes, the inherently reduced stability margin significantly increases both the likelihood and the impact of an event caused by the slight miscalculation in the roll induced by driving over a small rock. For machines which lift heavy loads, especially if they do so when operating on slopes, it becomes critical to understand the impact of the mass reconfiguration on overall stability.

Therefore, the capacity to measure instantaneous stability margin, to predict it in the near future, and to control it by choice of speed, articulation, and trajectory is a fundamental necessity for most classes of field robots if they are to be effective in realistic operational situations. It is well known that the realization of this capacity requires knowledge of the location of the center of gravity, the specific forces being experienced due to gravity and accelerated motion, and the geometry of the convex polygon formed by the wheel contact points with the terrain.

The literature has outlined how to use the tools of rigid body dynamics to define a useful threshold on proximity to tipover. Starting from this foundation, we investigate the unique issues associated with realization in the general case and then present a solution for a particular vehicle which approaches this general case in complexity.

1.2 Related work

Robotics adapted the study of vehicle stability from earlier studies of footfalls and gaits of animals [28]. The *support pattern* is defined as the convex hull in a horizontal plane which contains the vertical projections of the feet of all supporting legs. This concept was introduced to robotics early [23] from biomechanics [13] and it continues to be valuable. Based on this, early definitions of *stability margin* [24] involved the shortest distance from the projected cg to the sides of the support pattern.

Due to such roots, early work in robotics appeared in the context of walking machines [6,38]. Active control of the vehicle in order to maintain at least static stability has been a concern for even the earliest such vehicles [15] because the basic locomotion mechanism necessarily involves large changes in stability as legs are alternately lifted and dropped. Legged machines have also generally been targeted to rough terrain. This consideration and those of limited computation had caused early researchers to concentrate on the static case (with rare exceptions [31]).

Inspired in part by biological analogs, the desire to increase speeds led to the use of perception sensors like laser rangefinders [36] and structured light [25] to preview the terrain and hence predict future attitude. Body tilt affects the friction

required at footholds, but more fundamentally, the aggregate effect of gravity and kinematic acceleration must be known relative to the support pattern in order to assess the presence of unbalanced moments. The desire to accommodate rougher terrain led to the use of proprioceptive sensors to determine present attitude. In [19], for example, a vertical gyro and two oil-damped pendulums are used to indicate pitch and roll. While the response of the pendulums to lateral accelerations destabilized the controls in this work, such characteristics become valuable in our work as the basis of measuring rollover propensity in wheeled vehicles undergoing such accelerations.

Geometric expressions of stability were augmented by energy-based methods in [26]. Using the 3D positions of footholds, the support pattern was generalized to the *support boundary* and a straightforward calculation of the minimum impact energy required to statically destabilize the vehicle was developed. Contours of this *energy stability margin* served as a means to compute the optimum position of the center of gravity. This approach was realized in practice by our colleagues later in [46] on the Ambler rover and it was extended theoretically to include inertial and external loads in [11].

A second class of vehicles, the mobile manipulators, appear in the stability literature roughly a decade after legged machines. The main operational advantage of these devices – their lack of rigid attachment to the floor – comes only at the cost of surmounting the additional concern of preventing tipover when applying forces, lifting loads, or moving quickly. The speeds of early walking vehicles and the relatively small amount of mass that is articulated during individual leg movement made it possible to assume that the system cg was fixed in the body frame and that forces exerted on the body by manipulation dynamics could be ignored. However, since mobile manipulators are motivated by the movement of large masses, this issue became the first concern of related research. The key new ingredients of computing the cg location and using D’Alembert’s principle to assess the impact of dynamics appear early in [21] in the context of a hypothetical planar manipulator. This work also introduces the wheel lift off criterion for marginal stability which is an equivalent criterion to later angular measures, and it is similarly sensitive to cg height.

A stationary vehicle aggressively moving manipulators of 10% and 20% of its mass is studied in [7]. A planning algorithm is developed which uses full nonlinear dynamics of the multi-body system. First, limits on manipulation that preserve stability are computed and then optimal trajectories with respect those limits are generated. In an early attempt to actively enhance stability, Fukuda presents in [9] a concrete implementation that exploits the redundancy of mobile manipulators in order to position the cg. A resolved rate control mechanism is developed to drive both the end effector and the cg independently. Conditions of static stability are enforced so the manipulator and vehicle kinematic accelerations were presumably small enough to be ignored.

Sugano et al [41] develops a solution for mobile manipulators which accounts for dynamics of both the vehicle and the manipulator and any external forces by employing D’Alembert’s principle. The vertically projected position of the cg is replaced by the Zero Moment Point (ZMP) due to Vukobratovic [44]. This point

on the floor, where the resultant of moments of gravity, inertial forces and external forces vanish, is the point where a line through the net noncontact force vector pierces the support polygon.

A third class of vehicles, wheeled vehicles without manipulators, appears in the robotics stability literature concurrently with mobile manipulators. Shiller [37] takes a similar approach to [7] and applies it to moving wheeled vehicles by predicting lift-off on simulated smoothly varying terrain. Limits on tangential speed were derived that assure wheel lift-off would not occur. Tipover conditions are derived in terms of moments about the center of mass which are equivalent to defining a critical angle of the net specific force experienced at the cg.

Concerns of stability and traction introduce a direct tradeoff. Increased magnitude of contact normals generally occurs while the zero moment point approaches an edge of the support polygon. In [39] algorithms are developed to control both stability and traction while addressing the direct tradeoff between them. For what amounts to a hybrid legged/wheeled vehicle, the cg position is controlled by articulating the forks in such a way as to respect stability and traction limits. The authors describe a sensing suite that could be used to implement a realization in principle and demonstrate the algorithm in simulation. Later, in [17], these techniques are demonstrated on a Mars rover prototype and in [16] extended to include a Kalman Filter to determine wheel contact angles.

Papadopoulos et al [30] develop an improved measure of stability margin which like [37] expresses the margin for a given edge of the support polygon in terms of the angle between the net force acting at the cg and the normal to the associated edge. Intuitively, this measure amounts to the angle through which the net force must rotate in order to have zero moment about the associated axis. This angular form, like that of [26], has the desirable characteristic of being sensitive to the cg height. The angle is multiplied by the moment of the net force about the tipover axis, so it is also interpretable in terms of the work required to achieve instability. In related earlier work [32], these authors also develop a tipover prevention mechanism and verify it in simulation.

Of course, manufacturers of automobiles and industrial trucks have their own reasons to be interested in stability estimation. Early work in industry has concentrated on understanding the mechanics of the problem, [43,12,40,2,3,18,8,47] and analyzing accidents [14]. Simulators [10] and test programs [4] have been developed for evaluating vehicle designs in light of the influence of design parameters such as roll stiffness. More recently, the applicability of various sensors has been studied [35,20,45]. These developments generally do not address the case of mass articulation or even sensor processing. Clearly, the articulated case applies as much or more to industrial lift trucks, warehousing vehicles, cranes, excavators, etc as it does to mobile robotic manipulators. We can no doubt expect robotics to ultimately benefit from the intense commercial interest in suitable sensing that is occurring at this time.

1.3 Problem Statement

Having outlined a history of investigation going back four decades in robotics, we now observe that although the basic principles relevant to our problem had been outlined in nearly complete form long ago, the literature to date on this topic is dominated by abstract discussions of the relevant mathematics and physics. While such analysis admirably highlights the basics of the problem, there is much work to be done to address the challenges of practical applications in such an applied field as robotics. The problem addressed in the article is the concrete realization of a stability margin estimation system. It will turn out that we will also be able to produce an optional attitude reference by exploiting readily available sensing.

References to implementations on a real machine are rare in the literature, and when they occur, the discussion of the implementation has been limited to a brief mention of the sensors that were used. When sensors are mentioned, they are inclinometers and vertical gyros, used to sense a quasi-static situation on a very slow vehicle, or they are proposed sensors which while appropriate in principle, have not yet been validated. Estimation issues have been described so far only in the context of estimating wheel contact angles rather than the inertial forces which are central to stability margin estimation.

Many authors have used simulation to validate their concepts but there is no mention in these simulations of sensor modeling, noise and estimation techniques, compensation, numerical issues, computational efficiency, etc. Presumably, these works have not modeled the sensing process at all in their simulations – and the relevant dynamic quantities were read directly from the pristine simulator state. In short, little has been revealed so far in terms of appropriate sensing hardware and sensory processing techniques required to solve this problem on a real vehicle.

Thus, while the literature outlines how one assesses stability margin given the forces acting at the cg and their relationship to the support polygon, the computation of those forces, that of *stability margin estimation*, is an important problem in its own right. This problem has presumably been ignored so far due to the limited ambitions of contemporary fielded systems with regard to speeds, slopes, and payload articulations. Nonetheless, two CMU robots tipped over due to slopes and accelerated motion in 2004 (Fig. 1), so this problem is rapidly becoming relevant to field operations. As the article will outline, there are a large number of issues which arise immediately when one attempts to implement such a system. These issues are at times reminiscent of, and at times in stark contrast to, related issues arising in terrestrial inertial guidance and attitude estimation.

1.4 Discussion

By way of analogy to guidance, consider the following: the primary sensors used are specific force sensors (accelerometers and inclinometers). It is central to know that, despite the name, these devices do not measure acceleration. They measure the vector sum of kinematic acceleration and gravity by sensing the deflection of a restraint holding a mass. The mass cannot help but respond equally to kinematic acceleration



Fig. 1. Robot rollover events at CMU in 2004. [Left] The rough terrain vehicle "Yellow" shown suffered a 360 degree rollover due to soil failure on a long slope. [Right] The Grand Challenge vehicle called Sandstorm rolled during high speed testing due to several factors including high lateral acceleration during cornering.

and gravity – and this is a significant complication to guidance. Operation in both cases during accelerated motion requires the use of physical transformation laws to convert what is measured to what is desired. In guidance the motive is to remove apparent forces due earth spin and platform rotation. In stability estimation, the motive is to remove the inertial effects of any offset of the sensor frame with respect to the cg location. Doing so in both cases requires measurements of angular velocity of sufficient degrees of freedom to resolve the motions involved.

By contrast with guidance, consider the following: if the vehicle articulates any significant mass, the cg location must be computed in real time. This real-time mass properties calculation has no equivalent in guidance. The need to distinguish gravity from kinematic acceleration is one of the driving technical issues in inertial guidance. It leads to requirements to know the gravity field in which the system operates as well as the instantaneous vehicle attitude with respect to that field. For stability estimation, however, the response of specific force sensors to gravity is a virtue rather than a complication. Both forces have equal capacity to tip a vehicle and these devices conveniently measure the total effect of both in a coordinate system in which the support polygon is already known. It is not necessary to know gravity magnitude or attitude with respect to it to implement stability margin estimation. The vector sum of gravity and kinematic acceleration in the body frame provides sufficient information. This fact and the desire to compute forces rather than positions renders the problem quite solvable with less (or no) computing and less capable sensing.

The difficulty of using inertial sensors to compute position and attitude is well known in and outside of robotics [1,42,33,34]. However, stability estimation places new and significantly different requirements on sensing. In contrast to the high sensitivity of inertially computed position to sensor biases, stability margin is highly insensitive to it. In our problem, we are concerned only with the angle that the specific force vector at the cg takes with respect to tipover axes. This angle is,

by contrast, directly related to the sensor indications. Hence, an *uncompensated* accelerometer bias of one milli-g causes a constant instantaneous error of one milliradian in estimating specific force angle. In guidance, ignoring Schuler effects, the same bias causes an accumulating position error valued at 64 Km after an hour. In contrast to the double integration of specific force indications, we will find it necessary to perform single differentiation of the gyros, and double differentiation of the articulation sensors because our problem is partly one of computing kinematic acceleration from position rather than the reverse.

Despite the above statement that stability margin does not require knowledge of attitude, it is nonetheless possible to compute attitude from the same sensors given the terrain relative motion sensing (odometry) which is ubiquitous on mobile robots and many other vehicles. For this purpose only, accumulated bias effects must be regularly damped using conventional techniques. The sensor commonality also leads to situations where attitude estimation systems can assist in the computation of stability margin by making the strapdown specific force indications available to a stability module. Thus, specific force indications combined with odometry and bias compensation leads to attitude whereas their combination with physical transformation and articulation sensing leads to stability margin.

1.5 Approach

Given that estimating the specific force acting at the cg is the core problem in practice, our overall approach is as follows. Strapdown inertial sensing is mounted rigidly to the body in order to sense gross bodily motions relative to inertial space. These indications contain enough information to transform specific force to a moving cg frame of reference. Articulation sensing is used to compute the instantaneous location of the cg relative to the body. Stability margin is computed based on the transformed specific force and the support polygon. Attitude is computed from the same specific force readings by using terrain relative velocity in order to remove the kinematic acceleration component and reveal the gravity vector in body coordinates. The known gravity vector in the inertial frame then permits a solution for attitude.

The utility of a tipover proximity indicator is that it can be used to drive a number of mechanisms which can take corrective action. Autonomous systems can predict future proximity and modulate speed, curvature and load height to compensate. In the event of failure to do so correctly, an exception can be raised for resolution at higher levels of the autonomous hierarchy. For man-driven vehicles, a console indication or audible warning could be produced as a first measure. Alternately, or as a secondary measure, various governing mechanisms, such as travel speed or load height limiting, can be engaged to reduce the severity of the situation.

This article is organized as follows: Section 2 provides the definitions and assumptions used throughout this paper. Section 3 provides the physical principles involved in determining stability and attitude. Section 4 summarizes the classical approach used in this work to assessing the stability margin of the vehicle. Section 5 describes the test-bed used in testing the algorithms and Section 6 presents the opti-

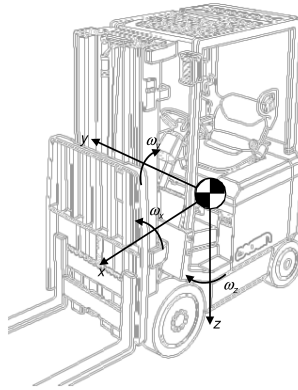


Fig. 2. SAE vehicle axis system.

mal estimation framework. Section 7 presents some results from the application of the algorithms presented in the paper.

2 Conventions and Notation

In this work we have adopted the SAE standard to define both the vehicle reference frame and its motion relative to an earth-fixed frame in a manner similar to that presented in [12].

Lumped mass. We will consider each part of the vehicle as a rigid body and each articulation as a rigid joint. The vehicle is treated as a rigid body and we use a single mass representation in which the vehicle is treated as a mass concentrated at its center of gravity (cg) (Fig. 2). The point mass at the cg with appropriate moments of inertia, is dynamically equivalent to the vehicle for all motions in which it is reasonable to assume the vehicle to be rigid.

Vehicle-fixed reference frame. The vehicle motions are defined with reference to a right-hand orthogonal reference frame which originates at the CG and travels with the vehicle. By SAE convention the coordinates are (Fig. 2) the following:

- x –Forward and on the longitudinal plane of symmetry
- y –Lateral out the right side of the vehicle
- z –Downward with respect to the vehicle
- ω_x –Angular velocity about the x axis
- ω_y –Angular velocity about the y axis
- ω_z –Angular velocity about the z axis

Motion variables. Vehicle motion will be described by the velocities (forward, lateral, vertical, roll, pitch, and yaw) with respect to the earth-fixed reference frame of a reference frame attached to the center of gravity.

Earth-fixed reference frame. Vehicle attitude and trajectory through the course of a maneuver are defined with respect to a right-hand orthogonal reference frame fixed on the earth, called $\{E\}$. It is normally selected to coincide with the vehicle-fixed reference frame at the point where the maneuver started. The coordinates are the following:

- X–Forward travel
- Y–Travel to the right
- Z–Vertical travel (positive downward)
- ψ –Heading angle (angle between x and X in the ground plane)
- θ –Pitch angle (angle between the vehicle x-axis and the ground plane)
- ϕ –Roll angle (angle between the vehicle y-axis and the ground plane)

Notation. The following notation is used throughout the paper.

- $\{a\}$ reference frame
- \vec{r}_b^a position of $\{b\}$ relative to $\{a\}$
- \vec{v}_b^a velocity of $\{b\}$ relative to $\{a\}$
- \vec{a}_b^a kinematic acceleration of $\{b\}$ relative to $\{a\}$
- $\vec{\omega}_b^a$ angular velocity of $\{b\}$ relative to $\{a\}$
- $\vec{\alpha}_b^a$ angular acceleration of $\{b\}$ relative to $\{a\}$
- ${}^a r_b$ position of $\{b\}$ relative to $\{a\}$ resolved in $\{a\}$
- ${}^a R_b$ rotation matrix describing $\{b\}$ relative to $\{a\}$
- ${}^a T_b$ homogeneous transform describing $\{b\}$ relative to $\{a\}$

When a vector lacks a superscript it will usually mean it is to be interpreted with respect to the inertial frame.

3 Physical Principles and Transformations

For our purposes it is expedient to assume that a frame of reference fixed to the surface of the earth is inertial. The largest error associated with this assumption is in the 10 milli-g range.

Transformation of inertial sensor measurement. With reference to Fig. 3, let frame $\{i\}$ be the inertial reference frame attached to the earth, frame $\{\sigma\}$ be a frame attached to an arbitrary sensor, and frame $\{c\}$ be attached to the cg of the vehicle. Two different $\{\sigma\}$ frames can be used to track the motions of inertial sensors and odometric sensors. The angular velocity of all frames mounted to the body is identical. The relative motion between the indicated frames is constrained as follows: $\vec{\omega}_\sigma^c = 0$, $\vec{v}_c^\sigma \neq 0$.

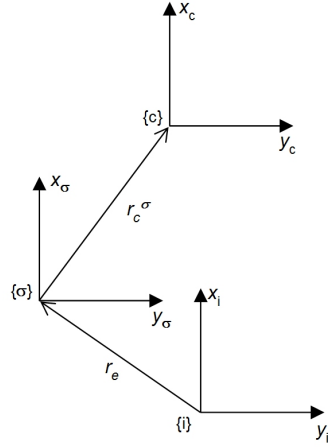


Fig. 3. Frames used in the transformation of sensor data.

Based on this reference frame arrangement we can express the position of the cg relative to the inertial frame, {i}, as follows:

$$\vec{r}_c^i = \vec{r}_σ^i + \vec{r}_c^σ \tag{1}$$

Taking the time derivative of Eq. 1 in the inertial frame, we obtain the velocity of the cg relative to the inertial frame:

$$\left(\frac{d\vec{r}_c^i}{dt}\right)_i = \left(\frac{d\vec{r}_σ^i}{dt}\right)_i + \left(\frac{d\vec{r}_c^σ}{dt}\right)_i \tag{2}$$

which simplifies to

$$\vec{v}_c^i = \left(\frac{d\vec{r}_c^i}{dt}\right)_i = \vec{v}_σ^i + \vec{v}_c^σ + \vec{\omega}_σ^i \times \vec{r}_c^σ \tag{3}$$

Taking the time derivative of Eq. 3 results in the kinematic acceleration relative to the inertial frame \$\vec{a}_c^i\$ of the cg determined, in part, from the readings of a sensor \$\sigma\$ positioned elsewhere (Eq. 4).

$$\vec{a}_c^i = \vec{a}_σ^i + \vec{a}_c^σ + 2\vec{\omega}_σ^i \times \vec{v}_c^σ + \vec{\alpha}_σ^i \times \vec{r}_c^σ + \vec{\omega}_σ^i \times \vec{\omega}_σ^i \times \vec{r}_c^σ \tag{4}$$

This can be written as:

$$\vec{a}_c^i = \vec{a}_σ^i + \Delta\vec{a}_c^σ \tag{5}$$

We have simply defined the last four terms of Eq. 4 as the kinematic acceleration increment $\Delta \vec{a}_c^\sigma$ needed to produce the cg acceleration from the sensor readings:

$$\Delta \vec{a}_c^\sigma = \vec{a}_c^\sigma + 2\vec{\omega}_\sigma^i \times \vec{v}_c^\sigma + \vec{\alpha}_\sigma^i \times \vec{r}_c^\sigma + \vec{\omega}_\sigma^i \times \vec{\omega}_\sigma^i \times \vec{r}_c^\sigma \quad (6)$$

This acceleration increment results from the location and motion of the cg relative to the sensor. Such induced inertial accelerations must be figured in the computation of cg motion. They are often denoted as follows:

Einstein acceleration	\vec{a}_c^σ
Euler acceleration	$\vec{\alpha}_\sigma^i \times \vec{r}_c^\sigma$
Coriolis acceleration	$2\vec{\omega}_\sigma^i \times \vec{v}_c^\sigma$
Centripetal acceleration	$\vec{\omega}_\sigma^i \times \vec{\omega}_\sigma^i \times \vec{r}_c^\sigma$

Specific force is defined as the vector difference of kinematic acceleration and gravity because a gravity vector pointing down and acceleration upward both tend to increase the specific force reading. The specific force reading of an accelerometer located at the origin of the arbitrary frame σ is therefore $\vec{t}_\sigma = \vec{a}_\sigma^i - \vec{g}$. Gravity is sensed identically independent of observer motion, so one can compute the specific force that would be measured by an accelerometer positioned at the cg of the vehicle by subtracting the gravity vector from both sides of Eq. 5 as follows:

$$\vec{t}_c = \vec{a}_c^i - \vec{g} = \vec{a}_\sigma^i + \Delta \vec{a}_c^\sigma - \vec{g} = \vec{t}_\sigma + \Delta \vec{a}_c^\sigma \quad (7)$$

Exposing the details for convenience, this is:

$$\vec{t}_c = \vec{t}_\sigma + \vec{a}_c^\sigma + 2\vec{\omega}_\sigma^i \times \vec{v}_c^\sigma + \vec{\alpha}_\sigma^i \times \vec{r}_c^\sigma + \vec{\omega}_\sigma^i \times \vec{\omega}_\sigma^i \times \vec{r}_c^\sigma \quad (8)$$

Character of stability estimation problem. Much of the character of the stability estimation problem, in all of its likely instances, can be deduced from the result in Eq. 8. Note first that gravity does not appear. The kinematic acceleration increment alone explains the difference in indications because both the real and hypothetical sensor respond to gravity identically. The quantity \vec{r}_c^σ vanishes only when the sensor is positioned at the cg. This case is important because it implies a computation-free solution when stability margin estimation can be designed in or retrofitted optimally on a non-articulating vehicle. In this case, even gyros or other angular velocity indications are unnecessary and the result operates correctly on rough terrain.

The quantities $\vec{\omega}_\sigma^i$ and $\vec{\alpha}_\sigma^i$ represent the rotational motion of the sensor with respect to the earth. On flat terrain, a single vertical axis gyro may be sufficient. Without a gyro, steer angle and/or wheel speeds can be used to compute it. On rough terrain three axes are needed for complete compensation. In any case, angular acceleration must be computed by numerical differentiation if the assumption of steady turning is not a good one.

The quantities \vec{v}_c^σ , and \vec{a}_c^σ represent the translational motion of the cg with respect to the sensor. The Coriolis and Einstein terms matter only on articulating vehicles. Both these derivatives will normally require numerical differentiation on an articulating vehicle employing conventional sensing (encoders, string pots). They are computed from the kinematics of the cg (Eq. 14) as indicated in the sequel.

Measurement model and attitude measurement. In the absence of a desire to compute attitude, Eq. 7 can be rearranged to produce a measurement model predicting the specific force indications from a sensor at any location given what would be measured by a hypothetical sensor positioned at the cg:

$$\vec{t}_\sigma^i = \vec{t}_c^i - \Delta\vec{a}_c^\sigma \quad (9)$$

However, it is possible to estimate attitude as well if gravity and kinematic acceleration are separated in the state vector. A slightly more complicated route is necessary in this case. Consider again the specific force at the sensor. By definition, it can be written in terms of its two components:

$$\vec{t}_\sigma^i = \vec{a}_\sigma^i - \vec{g} \quad (10)$$

Substituting from (Eq. 5).

$$\vec{t}_\sigma^i = \vec{a}_c^i - \Delta\vec{a}_c^\sigma - \vec{g} \quad (11)$$

This result is the basis of the measurement model for vector specific force used later. Note that \vec{t}_σ^i is the sensor readings, \vec{a}_c^i is computable from odometry sensing (e.g., wheel encoders or visual odometry,) and $\Delta\vec{a}_c^\sigma$ is the acceleration increment computed for stability estimation. Of course, wheel slip becomes more difficult to remove at high speeds and/or on rough terrain. GPS is a viable alternative when the required infrastructure (differential base station) can be supported, but reliable infrastructure-free terrain-relative velocity sensing under the most extreme such conditions is still an open problem.

Given odometry, all of these vectors are known in the coordinates of the body frame. Hence, the gravity vector *referred to body coordinates* can be computed. Once it is, the equation:

$${}^i\mathbf{g} = [0 \ 0 \ g]^T = {}^iR^b \mathbf{g} \quad (12)$$

can be solved for the attitude variables (pitch and roll) encoded in the rotation matrix relating the body and the inertial coordinate systems. While stability margin estimation requires specific forces at the cg, a sensor used only for attitude determination could be mounted anywhere. The cg frame above could be replaced with that of an odometry sensor for example.

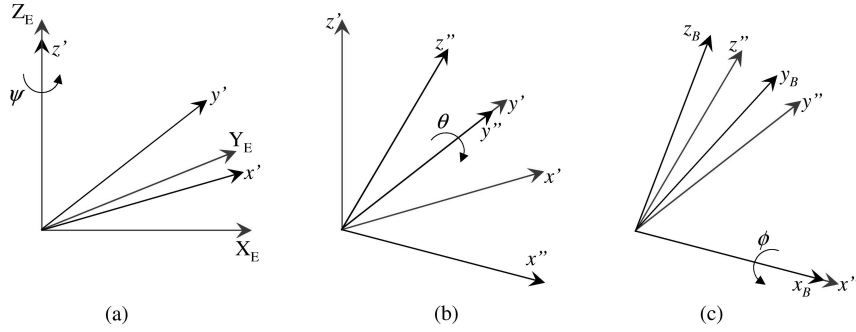


Fig. 4. Definition of the yaw ψ (a), pitch θ (b) and roll ϕ (c) angles based upon the ZYX-Euler angles.

Angular velocity. The relationship between the vehicle-fixed reference frame and the earth-fixed reference frame is defined by Euler angles. Euler angles are determined by a sequence of three rotations. Beginning at the earth-fixed reference frame, the axis system is first rotated in yaw (ψ), then in pitch (θ) and then in roll (ϕ) to line up with the vehicle-fixed reference frame (Fig. 4). The three angles obtained in this way are the ZYX-Euler angles.

The Euler angle rates $\dot{\psi}$, $\dot{\theta}$ and $\dot{\phi}$ are not directed along the axes x , y and z of the body frame and consequently do not coincide with the components ω_x , ω_y and ω_z of the angular velocity in the reference frame fixed to the vehicle (Fig. 2). Their directions are those of intermediate axes z_E , y' and x_B . Using this fact one can find these rates as a function of body angular rates from Eq. 13 as follows.

$$\begin{bmatrix} \dot{\phi} \\ \dot{\theta} \\ \dot{\psi} \end{bmatrix} = \begin{bmatrix} 1 & \frac{\sin(\theta) \sin(\phi)}{\cos(\theta)} & \frac{\sin(\theta) \cos(\phi)}{\cos(\theta)} \\ 0 & \cos(\phi) & -\sin(\phi) \\ 0 & \frac{\sin(\phi)}{\cos(\theta)} & \frac{\cos(\phi)}{\cos(\theta)} \end{bmatrix} \begin{bmatrix} \omega_x \\ \omega_y \\ \omega_z \end{bmatrix} \quad (13)$$

Kinematics of the CG. The center of gravity (cg) of the entire body-manipulator-payload system is the point at which the force of gravity can be considered to act and which undergoes no internal motion. For a given system configuration it is computed as the mass-weighted average position of every component where the computation is referred to a coordinate system fixed to the body frame.

$${}^B \mathbf{r}_c = {}^B T \left({}^0 \mathbf{r}_{c_0} m_0 + \sum_{i=1}^n \left(\prod_{j=1}^i {}^{j-1} T (\Theta_j) \right) {}^i \mathbf{r}_{c_i} m_i \right) \frac{1}{m} \quad (14)$$

Eq. 14 defines the instantaneous location of the cg (${}^B \mathbf{r}_c$) as a function of joint variables Θ_j , the masses of the individual bodies composing the vehicle (m_i) and

the total mass of the vehicle (m). The location of the cg relative to an arbitrary sensor frame $\{\sigma\}$ can be computed from the location of the cg through the application of:

$${}^{\sigma}\mathbf{r}_c = {}^{\sigma}T^B \mathbf{r}_c \quad (15)$$

4 Assessment of stability margin

Once the specific forces acting at the cg are known, assessing stability margin is accomplished by relating them to the geometric footprint or (*support polygon*) of the vehicle. Vehicle stability margin is defined here in a manner consistent with the force-angle measure proposed by Papadopoulos and Rey [29]. The following material is adapted from the cited work for the sake of completeness of the exposition.

For a general mobile robot the polygon of support is defined by the robot contact points with the ground which form a *convex polygon* when projected onto the horizontal plane. For example, in a wheeled vehicle these contact points may be defined by the center of the contact patch of each tire and the ground surface. Let \vec{r}_i represent the location of the i -th ground contact point and let \vec{r}_c represent the location of the vehicle center of mass. As illustrated in Fig. 5 these vectors can be expressed in the vehicle frame $\{B\}$ and numbered such that the unit normal of the support polygon is directed upward and out of the ground. The boundary of the support polygon is defined by the lines joining the ground contact points. These lines are the candidate tipover axes, $\vec{a}_i, i = 1 \dots n$. The i -th tipover axis is the axis about which the vehicle will physically rotate during a tipover event; it defines the normal to the *tipover plane* (Fig. 5). The tipover plane serves as a simplification onto which the vehicle mass properties and the forces acting on the vehicle are projected in order to analyze the tipover propensity about the plane normal.

The process used to formulate the stability measure can be understood intuitively in terms of the direction in which an imaginary pendulum would deflect if it were positioned at the center of gravity. The forces such a pendulum would experience include gravity and the inertial force due to its accelerated motion with respect to the earth. At the point where lift off is about to occur, all terrain forces either vanish or they have no moment about the tipover axis under consideration.

At the center of gravity, the sum of real forces acting on the vehicle generates the inertial force ($\vec{f}_{\text{inertial}}$). The real forces include the gravitational loads (\vec{f}_g), ground reaction forces at the vehicle's wheels (\vec{f}_s), and any other external disturbances acting on the vehicle (\vec{f}_d). The dynamic force equilibrium equation can be written as in Eq. 16.

$$\sum \vec{f}_{\text{inertial}} = \sum (\vec{f}_g + \vec{f}_s + \vec{f}_d) \quad (16)$$

The net force acting on the cg that would contribute to tipover instability about any tipover axis, \vec{f}_r , is defined in Eq. 17.

$$\vec{f}_r \triangleq \sum (\vec{f}_g + \vec{f}_d - \vec{f}_{\text{inertial}}) = - \sum \vec{f}_s \quad (17)$$

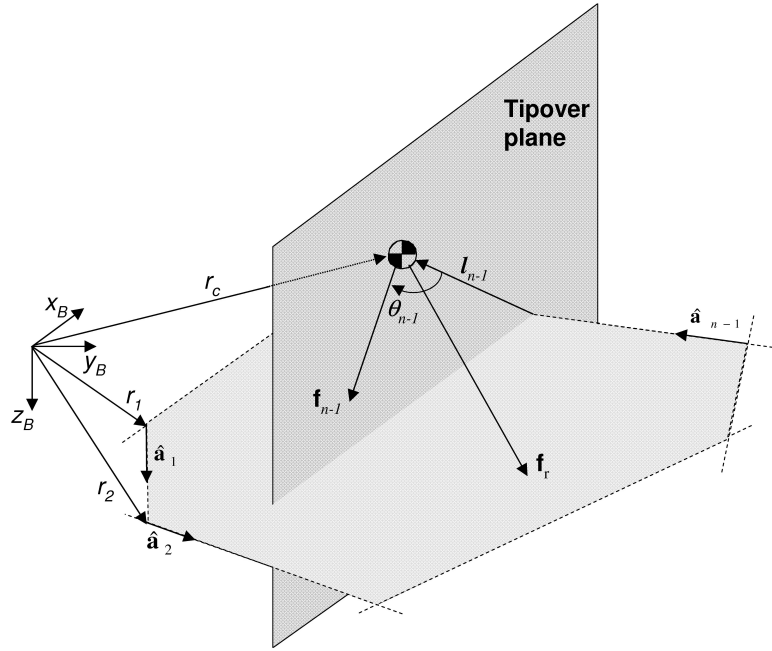


Fig. 5. Assessment of dynamic stability

For a given tipover axis \vec{a}_i , we are only concerned with those components of \vec{f}_r which act *about* the i -th tipover axis. The projection of the resultant force onto the i -th tipover plane and the moment of the resultant force about the plane normal are used to compute the stability measure as follows.

Let \vec{f}_i be the projection (e.g., the component of \vec{f}_r acting along the i -th tipover axis) of the resultant force onto the tipover plane. Then

$$\vec{f}_i = \vec{f}_r - (\vec{f}_r \cdot \hat{a}_i) \hat{a}_i \quad (18)$$

and $\hat{a}_i = \vec{a}_i / |\vec{a}_i|$. Similarly, the torque acting about the i -th tipover axis can be computed from Eq. 19.

$$\vec{n}_i = \left((\vec{l}_i \times \vec{f}_r) \cdot \hat{a}_i \right) \hat{a}_i \quad (19)$$

In Eq. 19, \vec{l}_i is the i -th tipover axis normal given by

$$\vec{l}_i = (\vec{r}_i - \vec{r}_c) - \left((\vec{r}_i - \vec{r}_c) \cdot \hat{a}_i \right) \hat{a}_i \quad (20)$$

The stability measure for each tipover axis is defined as the subtended angle between the i -th resultant force, \vec{f}_i , and the i -th tipover axis normal, \vec{l}_i , as illustrated in Fig. 5. This measure is denoted by θ_i and can be computed from Eq. 21 as follows:

$$\theta_i = -\arcsin\left(\frac{(\vec{l}_i \times \vec{f}_i) \cdot \hat{a}_i}{|\vec{l}_i| |\vec{f}_i|}\right) \quad (21)$$

The stability margin with respect to a given tipover axis is determined from the value of the corresponding resultant angle as follows. If the resultant angle $\theta_i > 0$ the vehicle is stable about the i -th tipover axis. If $\theta_i = 0$ the vehicle is marginally stable about that tipover axis. This means that the ground reaction forces at the inside support points relative to the i -th tipover axis are zero. If $\theta_i < 0$ the vehicle is critically stable, meaning that it is experiencing an unbalanced tipover moment about the i -th tipover axis. The overall stability margin of the vehicle is defined by Eq. 22.

$$\theta = \min(\theta_i) \quad (22)$$

5 Real and Simulated Test-beds

The test-bed selected to exercise the stability prediction algorithm is a commercial lift truck designed for warehousing applications. Although such vehicles rarely operate on rough terrain, they do operate on ramps and many routinely move and turn when their centers of gravity are placed at heights several times the width of the vehicle. Such vehicles have static tipover thresholds expressed in projected gravity ranging from 0.1 to 0.54 g whereas equivalent thresholds for a 70 inch wide over-the-road truck are 0.4-0.6 g [12]. In order to measure the physical quantities required by the algorithm, the sensors used in the test bed included inertial, odometric, and articulation sensors.

Motivations for the test-bed construction included sensor comparisons aimed at characterizing and producing a low cost solution. Therefore, a commitment was made early to a single axis of gyro sensitivity but for both gyros and accelerometers, redundant high end sensing was employed in order to serve as rough ground truth for the inexpensive sensing. All sensors were integrated in a Kalman filter configured for intermittent measurement availability to permit such comparisons relatively easily.

Overall sensing requirements for the problem can be classified in terms of articulation sensing necessary to measure cg motion in the body frame and sensing for the motions of the body relative to the earth. Stability estimation requires indications of the direction (not necessarily magnitude) of specific force. These can be obtained from inclinometers or accelerometers – which are only different packages for the same measurement principle. Angular velocity must be measured in order to compensate for apparent forces when the specific force sensors are not at the cg, or in order to disambiguate kinematic acceleration from gravity in order to determine

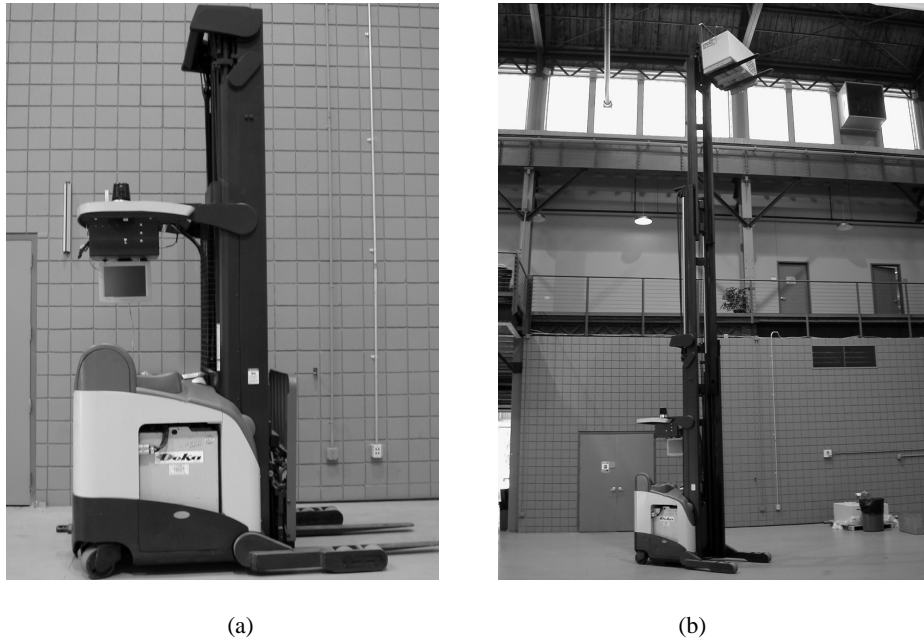


Fig. 6. Vehicle test bed. In (b) the mast is extended to 340 inch high resulting in a cg height of 182 inch with a 4500 lbs load.

attitude. This can be generated from gyros, from differential wheel speeds, from speed and curvature (steer angle) sensing, or from gyros and curvature sensing. Note that there is no fundamental need to measure ground relative translational motions except when determining attitude.

During development and testing, two implementations of the test-bed platform were used: hardware and simulation. The hardware platform is shown in Fig. 6. This lift truck underwent major retrofitting to incorporate the sensor suite used in the system. The computing platform is a general purpose 3U form factor 8-slot chassis containing a backplane for PXI and Compact PCI modules. The CPU module is a National Instruments PXI-8170 series consisting of a 850 MHz Pentium III processor with 256 MB of memory. The sensors include the BEI GyroChip QRS11 gyro, the Analog Devices ADXL105 3 axis accelerometer, and the Applied Geomechanics 758 Series inclinometer.

The mechanical design of this lift truck provides for two outriggers each having two caster wheels. Two more wheels are mounted in the back for which one of them provides traction and steering. This wheel configuration produces a polygon of support with six sides (a_1, \dots, a_6) as illustrated in Fig. 7. Each of the edges on this convex polygon are candidate tipover axes. As a result, this vehicle has six resultant angles $\theta_1, \dots, \theta_6$.

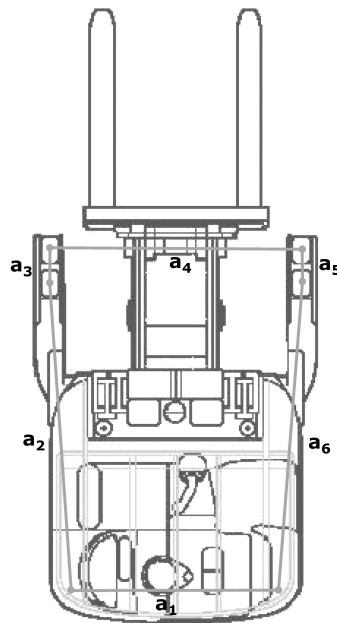


Fig. 7. Support polygon for the test bed.

As part of the hardware platform, a data logger system was developed. The main function of the logger is to provide input data to the system from either the vehicle sensors, from previously generated log files or from simulated sensor data. In the design of the logger, care was taken to guarantee deterministic log playback to ensure identical system response regardless of the source of the input data.

Like many authors before us who have addressed this topic, we have invested in simulation in part because we are developing systems that function when vehicles are operated near their stability limits. It is considerably more difficult to conduct an entirely experimental development program for such systems than it would be for algorithms intended for nominal vehicle operating conditions. Our test bed results in less challenging maneuvers are therefore augmented by simulation results for more aggressive maneuvers.

The simulation environment consists of two major components: 1) a high fidelity dynamic model of the truck and 2) a sensing/driver control system. The dynamic model is a 21 degree of freedom rigid body dynamic model of the truck which has been developed in the commercial simulation package ADAMS [27] (Fig. 8). The sensing/driver control system was developed in Matlab/Simulink and included models for inertial sensors and a user interface to simulate input driver commands to the truck including steer, speed, lift height, side-shift and tilt. Furthermore a software interface layer was defined to connect the stability prediction algorithms to the sensing system. This interface was created so that the implemented stability



Fig. 8. Rigid body dynamic model of the test bed.

prediction algorithms would require no changes and would be unaware of whether they were running on the hardware platform or on the simulation environment.

Through the driver control interface the user can input drive commands to the truck which results in the dynamic model responding to these input commands. As the vehicle executes the user commands the sensing system monitors the stability of the truck. This operational mode duplicates the operational mode of the hardware platform providing a rich environment for testing and debugging of the algorithms.

6 Optimal estimation framework

We present below an optimal estimation framework designed for stability margin estimation for a commercial lift truck. The estimation and prediction system is based on an extended Kalman filter (EKF) [22]. At the outset several sensor suites were considered including a set of force sensors at the wheels which might predict the point of lift-off more-or-less directly. We opted ultimately for a solution based on inertial sensing due to its presumed higher robustness to terrain irregularities.

While the primary purpose of the work is to develop stability estimation algorithms, it became clear early that a simple reformulation of the filter would permit the simultaneous extraction of vehicle attitude as discussed earlier. Given this design decision, it becomes natural to formulate a state vector which encodes the motion of

the cg in inertial space and the attitude of the vehicle. If our only purpose were stability margin estimation, specific force states would be more appropriate unless we were willing to assume the vehicle was always level before lift-off of a wheel. Similarly, if our only purpose were attitude determination, articulation and the location of the cg would not be material.

Due to the quest for a low cost solution the filter is based on a single axis of gyro sensitivity – around the body vertical axis – and we choose to accept that compensations for some inertial forces will be inexact during roll and pitch motions. When a 3 axis gyro is available, the more general case can be constructed using Eq. 13. Our test results verify that the instantaneous errors induced by this effective assumption (that the other two axes of rotation rate are zero) are removed as soon as these motions are over. There is no enduring effect on the attitude estimate because gravity indications project directly onto attitude states.

The overall structure is a two-tier Kalman Filter design. Tier 1 runs while the vehicle is stationary and Tier 2 runs while the vehicle is in motion. Tier 1 utilizes a bank of linear Kalman Filters (one per inertial sensor) with each filter implementing a random walk process model with given process noise [22]. When the vehicle is stationary this bank of Kalman filters computes the biases of all inertial sensors. Tier 2 implements the extended Kalman filter presented below and removes the sensor biases computed in Tier 1 during vehicle motion.

6.1 System Dynamics

The system's state vector describes the motion of the cg of the vehicle as well as the vehicle attitude:

$$\mathbf{x} = [\mathbf{v} \ \mathbf{a} \ \omega_z \ \alpha_z \ \phi \ \theta]^T \quad (23)$$

where \mathbf{v} and \mathbf{a} are the linear velocities and accelerations of the cg with respect to the earth-fixed reference frame (assumed to be inertial), ω_z and α_z are the angular velocities and accelerations with respect to the inertial frame of a frame fixed to the cg projected onto the body z-axis, and ϕ and θ are the Euler angles that describe the vehicle attitude. Furthermore, due to the rigidity of the suspension system in the class of vehicles considered here, we assume that the Euler angles are a direct description of terrain inclination in the lateral and longitudinal directions.

Using the definitions of $\dot{\phi}$ and $\dot{\theta}$ given in Eq. 13 the system dynamics can be described by the following differential equation:

$$\dot{\mathbf{x}} = \mathbf{f}(\mathbf{x}) = \left[\mathbf{a} \ \mathbf{0}_{3 \times 1} \ \alpha_z \ 0 \ \frac{\sin(\theta) \cos(\phi) \omega_z}{\cos(\theta)} \ -\sin(\phi) \omega_z \right]^T \quad (24)$$

This system model is nonlinear. We linearize it according to the rules for an extended Kalman filter. That is, we linearize it about the current estimate of the state:

$$\Delta \dot{\mathbf{x}} = \left. \frac{\partial \mathbf{f}}{\partial \mathbf{x}} \right|_{\mathbf{x}=\hat{\mathbf{x}}_k^-} \Delta \mathbf{x} \quad (25)$$

The system Jacobian $F = \left. \frac{\partial f}{\partial x} \right|_{x=\hat{x}_k^-}$ is defined in Eq. 26.

$$F = \left[\begin{array}{cccccc} \mathbf{0}_{3 \times 3} & \mathbf{1}_{3 \times 3} & \mathbf{0}_{3 \times 1} & \mathbf{0}_{3 \times 1} & \mathbf{0}_{3 \times 1} & \mathbf{0}_{3 \times 1} \\ \mathbf{0}_{3 \times 3} & \mathbf{0}_{3 \times 3} & \mathbf{0}_{3 \times 1} & \mathbf{0}_{3 \times 1} & \mathbf{0}_{3 \times 1} & \mathbf{0}_{3 \times 1} \\ \mathbf{0}_{1 \times 3} & \mathbf{0}_{1 \times 3} & 0 & 1 & 0 & 0 \\ \mathbf{0}_{1 \times 3} & \mathbf{0}_{1 \times 3} & 0 & 0 & 0 & 0 \\ \mathbf{0}_{1 \times 3} & \mathbf{0}_{1 \times 3} & \frac{\sin(\theta) \cos(\phi)}{\cos(\theta)} & 0 & -\frac{\sin(\theta) \sin(\phi) \omega_z}{\cos(\theta)} & \frac{\cos(\phi) \omega_z}{\cos^2(\theta)} \\ \mathbf{0}_{1 \times 3} & \mathbf{0}_{1 \times 3} & -\sin(\phi) & 0 & -\cos(\phi) \omega_z & 0 \end{array} \right]_{x=\hat{x}_k^-} \quad (26)$$

Given the initial condition $x = x_k$ at time t_k we approximate the solution of the system of ordinary differential equations (Eq. 24) at time $t_{k+1} = t_k + dt$ using the formula for the Euler method (Eq. 27).

$$x_{k+1} = x_k + f(x_k) dt \quad (27)$$

This is a first order discrete series approximation to the real function with dt being the time between samples. Higher order ordinary differential equation solvers could be applied (e.g., Fourth order Runge-Kutta), however they require large number of function evaluations and may not meet the real-time requirements imposed on the update loop of the filter. To ensure that the solution is stable and with a bounded error, the update loop of the Kalman Filter is run at twice the rate of the fastest sensor in the system.

6.2 Measurements

We are interested in the true motion of the cg because that motion determines the instantaneous stability margin of the vehicle. However, sensor indications describe the sensor's own motion. To find the true cg motion, sensor indications must be mapped onto equivalent indications at the cg taking into account the motion of the cg relative to the sensor. However, in a Kalman filter context, the relevant models are forward models. We therefore compute in the measurement models, the predicted sensor readings in the sensor frames of reference given the current value of the state and the filter machinery will invert these relationships for us to determine the true cg motion.

Measurement model. For this vehicle, the measurement vector z includes (Eq. 28): yaw rate gyro (ω), steer encoder (δ), speed encoder (v), accelerometers specific force (t), roll (Φ) and pitch (Θ) inclinometers. The accelerometers and inclinometers are redundant indications of specific force — introduced in order to evaluate their relative merits.

$$z = [z_\omega \ z_\delta \ z_{v_x} \ z_{v_z} \ z_{t_a} \ z_\Phi \ z_\Theta]^T \quad (28)$$

Eq. 29 gives the relationship between the state (x) and measurement (z) vectors which is non-linear. The measurement Jacobian is defined as $H = \frac{\partial h}{\partial x}$ and the

matrix ${}^i_B R = R_z(0) R_y(\theta) R_x(\phi)$ is the ZYX-Euler angles rotation matrix that describes the orientation of the vehicle relative to the earth, and ${}^B_i R = {}^i_B R^{-1}$. Many earlier equations are written in terms of a generic sensor frame of reference denoted by the letter (σ) but the implementation requires the distinction of several sensors which are positioned throughout the vehicle. In the following, the letter 'e' refers to a frame fixed to the wheel encoder, the letter 'a' refers to a frame fixed to the accelerometer cluster and the letter 'd' refers to a frame fixed to the steer encoder. The letter 'c' continues to refer to a frame fixed to the cg.

$$h(x) = \begin{bmatrix} \arctan\left(\frac{\omega_z}{\frac{v_y - v_{c_y}^\delta - \omega_z r_{c_x}^\delta}{v_x - v_{c_x}^\delta + \omega_z r_{c_y}^\delta}}\right) \\ v_x - v_{c_x}^e + \omega_z r_{c_x}^e \\ v_z - v_{c_z}^e \\ \mathbf{a} - {}^B_i R \mathbf{i} \mathbf{g} - \Delta \vec{\mathbf{a}}_c^a \\ \arctan\left(\frac{-({}^B_i R \mathbf{i} \mathbf{g} - \Delta \vec{\mathbf{a}}_c^a)_y}{({}^B_i R \mathbf{i} \mathbf{g} - \Delta \vec{\mathbf{a}}_c^a)_z}\right) \\ \arctan\left(\frac{({}^B_i R \mathbf{i} \mathbf{g} - \Delta \vec{\mathbf{a}}_c^a)_x}{({}^B_i R \mathbf{i} \mathbf{g} - \Delta \vec{\mathbf{a}}_c^a)_z}\right) \end{bmatrix} \quad (29)$$

The measurement Jacobian is omitted due to its complexity but it can, of course, be derived from the above. Note that the models for the specific force sensors involve the vehicle attitude so the filter will update vehicle attitude and compensate for inertial effects continuously during even accelerated motions.

6.3 Articulation Derivatives

The velocity (\vec{v}_c^σ) and acceleration (\vec{a}_c^σ) of the cg relative to an arbitrary sensor frame $\{\sigma\}$ are computed by numerically differentiating Eq. 15 as follows. Let $[\sigma \mathbf{r}_c] : [t_{k-\nu} \dots t_k] \rightarrow {}^\sigma_B T^B \mathbf{r}_c$ be a discrete function on the subdomain of ${}^\sigma \mathbf{r}_c$ from time $t_{k-\nu}$ to time t_k . The numerical derivative of $[\sigma \mathbf{r}_c]$ at time t_k is evaluated on an n degree interpolating polynomial \mathcal{P} (Eq. 30) computed from a weighted least squares approximation to $[\sigma \mathbf{r}_c]$. The polynomial \mathcal{P} is constructed from the sequence of orthogonal polynomials P_0, P_1, \dots, P_n with respect to the discrete weighted inner product of Eq. 31 where W is a m -vector of positive weights to be used, and m is the number of discrete points in the domain of $[\sigma \mathbf{r}_c]$. To complete the description of \mathcal{P} , the coefficients $D_j, j = 1 \dots n + 1$ are computed from Eq. 32 [5].

$$\mathcal{P}(x) = D_1 P_0(x) + D_2 P_1(x) + \dots + D_n P_{n-1}(x) + D_{n+1} P_n(x) \quad (30)$$

$$\langle P, Q \rangle = \sum_{x=1}^m P(x) Q(x) W(x) \quad (31)$$

$$D_{j+1} = \frac{\langle [\sigma \mathbf{r}_c], P_j \rangle}{\langle P_j, P_j \rangle}, j = 0, \dots, n \quad (32)$$

7 Results

The experiments performed to verify the functionality of the system involved driving the vehicle on ramps and level ground. Different maneuvers were executed, e.g., constant curvature/constant speed/changing load location, constant curvature/variable speed, and variable curvature/variable speed. Testing on ramps was important to verify that the system was able to correctly estimate terrain grade. For the test trajectories described above, the system was able to estimate the attitude of the vehicle (i.e., terrain grade) to within two degrees during accelerated motions of relatively short duration. An automatic zero velocity update procedure based on the bias estimation algorithm described earlier allowed us to measure and remove sensor biases regularly when the vehicle came to a stop to pick or drop a load.

Two different experiments are presented below: a constant curvature/variable speed case, and a variable curvature/variable speed case. For both, the vehicle carried a load of 3000 lbs while executing the drive commands.

Case A: Constant curvature/Variable speed For the first experiment the vehicle was commanded to follow a trajectory that included a straight line segment followed by a high curvature segment with increasing speed (Fig. 9). The trajectory and the input drive commands are shown in Fig. 10 and Fig. 11. For this maneuver the maximum commanded vehicle speed is 10 m.p.h. The sensor inputs to the stability prediction algorithm are shown in Fig. 12-a while the outputs of the stability prediction system are shown in Fig. 12-b, Fig. 13-a and Fig. 13-b.

As the vehicle travels in the high constant curvature path, the longitudinal velocity of the truck is increased from 2.5 m.p.h to 10 m.p.h.. This causes an increase in lateral acceleration (as illustrated in Fig. 12-b by a_y). As a result, the resultant angles that correspond to the outside tipover axes decrease to a point where the truck has reached marginal stability: the resultant angle (θ_2) in Fig. 13-b moves toward zero and crosses a stability threshold. When any of these angles reaches the point of marginal stability all the commands that are likely to contribute to decreasing vehicle stability are disabled (Fig. 13-a). In this case the velocity, lift and side-shift commands are disabled. As a result, the vehicle velocity reaches a maximum of 6 m.p.h even though the maximum commanded speed was 10 m.p.h: the stability prediction algorithm computed the maximum vehicle speed that will keep the vehicle in a stable region.

Furthermore, as the vehicle travels in the high curvature path with increasing velocity the roll and pitch inclinometers (Fig. 12-a) are unable to decouple the centripetal acceleration from gravity, as indicated by the high values of the roll and pitch angles. On the other hand the estimate for the roll and pitch angles of the vehicle (which gives an estimate of the terrain grade) remain within 2 deg which corresponds to the fact that the vehicle is traveling on flat terrain.

An independent method of detecting the tipover event was constructed in order to verify the detection algorithm. We equipped the high fidelity dynamic model with simulated sensors that could measure reaction forces at the wheels. We then verified that our detector indicates zero stability angles at precisely the same time that the

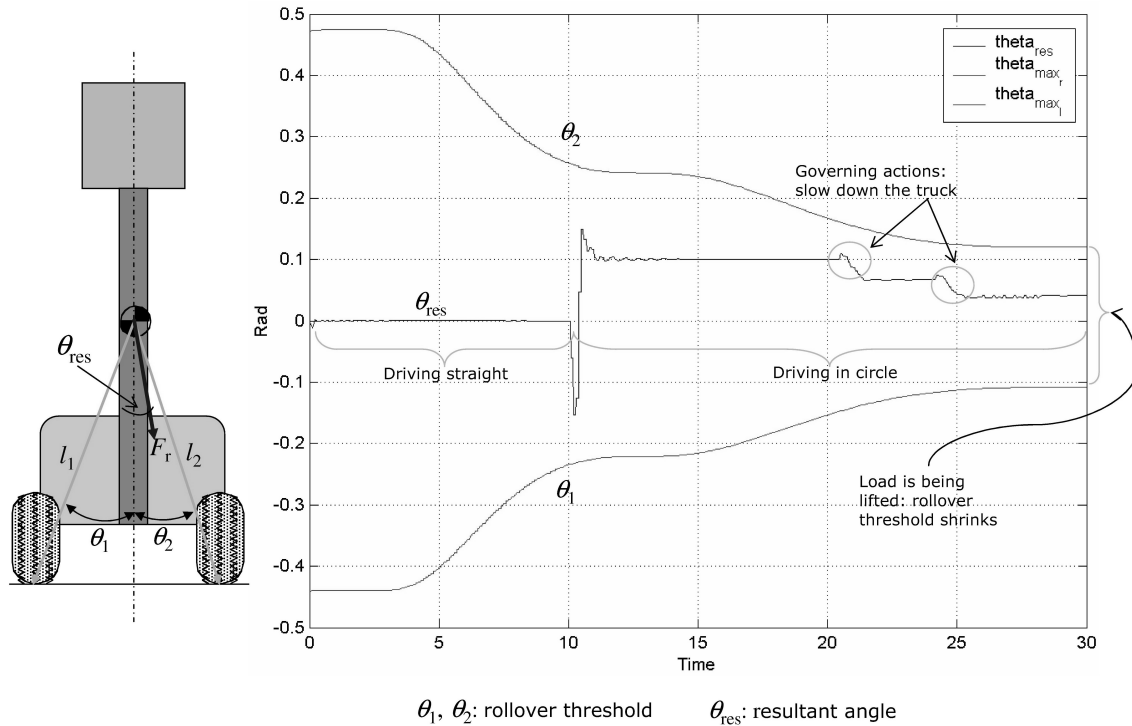


Fig. 9. Conceptualization of right (θ_1) and left (θ_2) tipover angles as a function of time. As the load is lifted the tipover angles decrease up to a point where the angle of the resultant force (θ_{res}) is close to the right tipover angle. This happens when the resultant force (f_r) passes through the contact point for tipover axis normal l_2 .

simulated wheel sensors read vanishing reaction forces. As illustrated in Fig. 14, the wheel reaction forces on the inside wheels approaches zero. For this vehicle that happens when the caster wheel (which is one of the inside wheels in this example) lifts off. In Fig. 14 the caster wheel reaction force approaches zero but reaches a safe minimum at the time when the governing actions take place.

Case B: Variable curvature/Variable speed For the second experiment the vehicle was commanded to follow a trajectory with variable curvature and variable speed (0 to 6.5 m.p.h.). For reference, the trajectory and the input drive commands are shown in Fig. 15 and Fig. 16, the sensor inputs to the stability prediction algorithm are shown in Fig. 17-a, while the outputs of the stability prediction system is shown in Fig. 17-b and Fig. 18.

As the vehicle travels in the specified path the vehicle speed is increased to 6.5 m.p.h. This causes an increase in lateral acceleration (Fig. 17-b)) which generate a

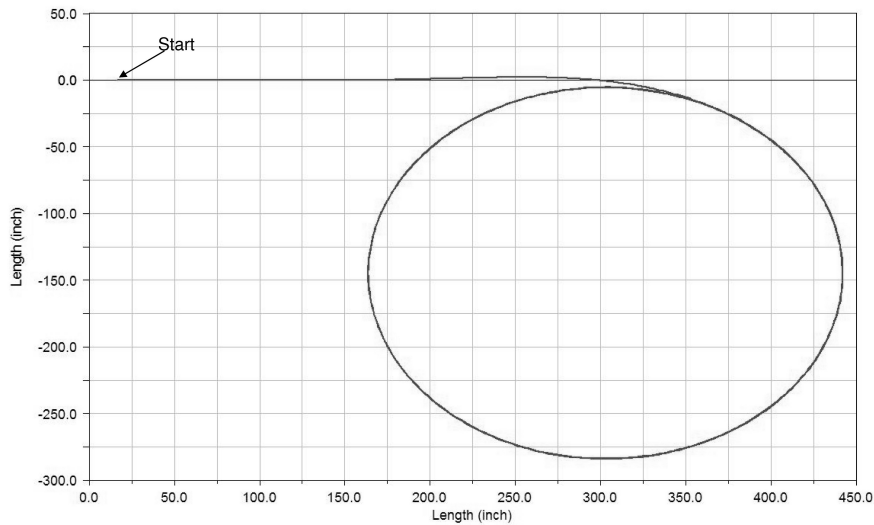


Fig. 10. Case A: Vehicle trajectory.

decrease in the resultant angles associated with the outside wheels (Fig. 18). In this case the candidate tipover axes change as the vehicle's path changes curvature. As with the previous example, when any of these angles reached the point of marginal stability, all the commands that are likely to make the situation worse are disabled.

Furthermore, as the vehicle travels the specified path the roll and pitch inclinometers (Fig. 17-a) are unable to decouple the centripetal acceleration from gravity, as indicated by the high values of the roll and pitch angles. On the other hand the estimate for the roll and pitch angles of the vehicle remain within 2 deg which corresponds to the fact that the vehicle is running on flat terrain.

8 Conclusions

The article has posed the stability margin estimation problem in the fairly general form of an articulating vehicle undergoing accelerated motions and described a concrete realization of a solution. The solution to stability margin estimation is highly compatible with but independent of the solution to attitude determination. Hence, one can determine attitude from the same sensors although attitude is not needed to estimate stability margin and the basic compensation calculation of apparent forces is identical to both problems.

Key elements of the approach to stability margin estimation include explicit models of mass articulation, explicit compensation for inertial forces, and an optimal estimation framework. For attitude determination, key elements include a formulation that determines the inertial motion of the cg frame of reference, and the use of odometry in order to support the disambiguation of kinematic acceleration and

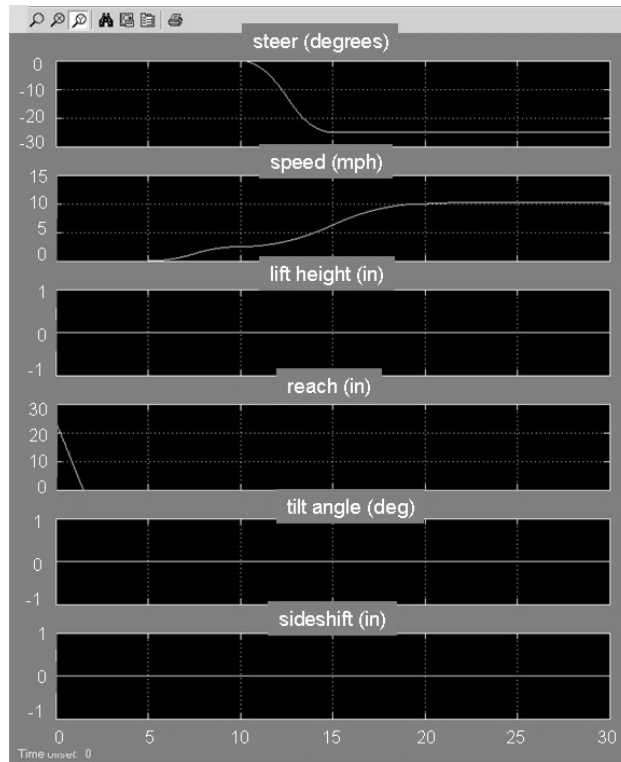
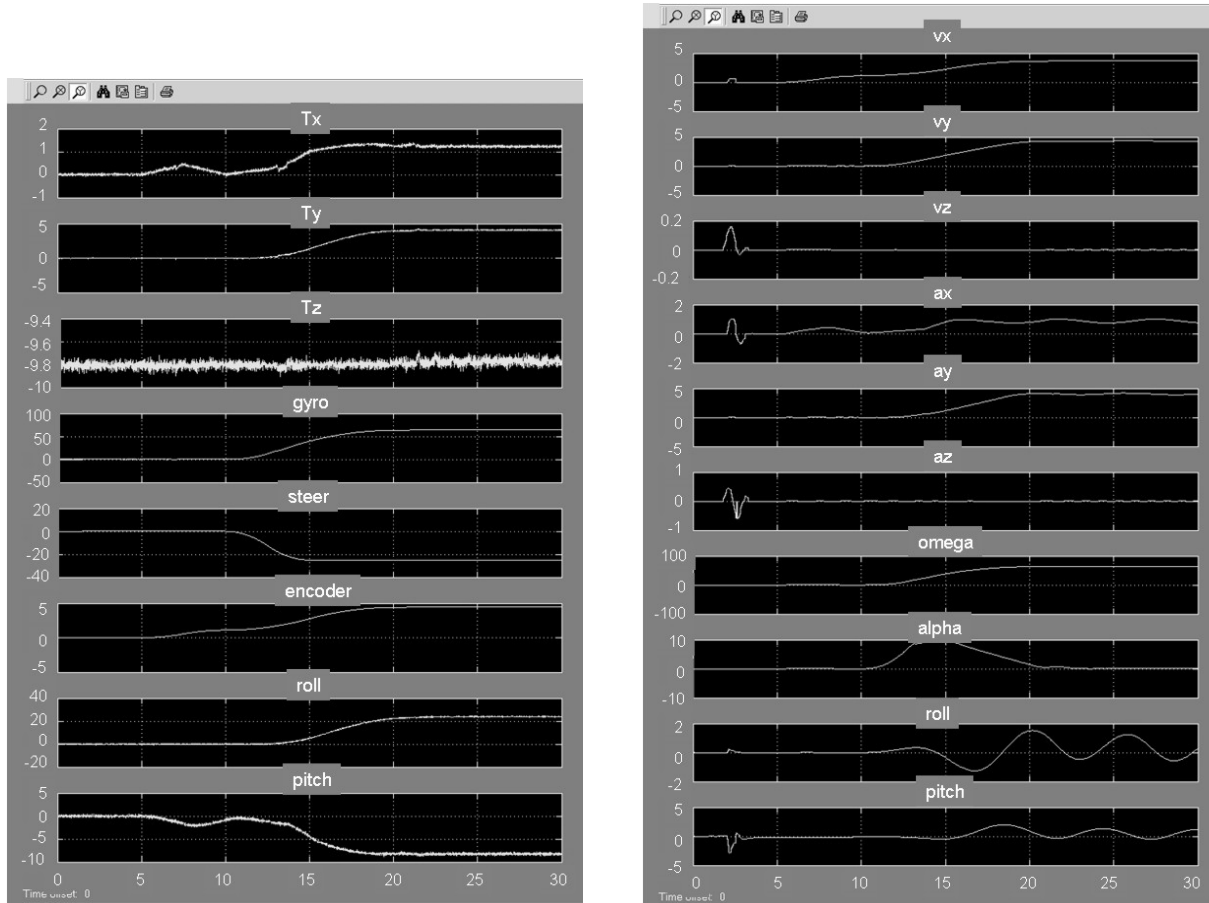


Fig. 11. Case A: Drive inputs.

gravity. The generality of the approach makes it potentially relevant to a broad class of indoor and outdoor material handling and excavation vehicles whether they are man-driven or robotic. The system could form the basis of a governor which discourages aggressive driving for man-driven vehicles, or one that implements a low level reactive control system for an autonomous vehicle that seizes control when higher level intelligence has underestimated the risk level in its predictive calculations.

The key design issues in practical solutions to the stability margin estimation problem arise due to the offset position of the sensing from the cg. In rare situations, it may be possible for an essentially unarticulated machine to place sensing near enough to the cg to be able to implement stability estimation for even rough terrain in little or even no computation. For machines that articulate or ones for which arbitrary sensor placement is not possible, the techniques of the article have been demonstrated to produce a practical result in reasonable effort. In future, as guidance systems become less expensive, it is more likely that stability prediction will be implemented as a computational layer over these existing sensors or even that such functionality will become embedded in the guidance system itself. However the solution is packaged, it seems inevitable that autonomous and man-driven vehicles of all kinds will shortly



(a)

(b)

Fig. 12. Case A: (a) Simulated sensor indications. Tx, Ty, and Tz represent accelerometer specific force. Roll and pitch are the outputs of the simulated inclinometers. As the vehicle travels the constant curvature path the roll inclinometer is unable to differentiate between gravity or inertial acceleration due to motion. (b) Vehicle cg state. As the vehicle enters the constant curvature path, lateral velocity and acceleration are being estimated. Lateral acceleration is used in the stability measure to monitor the lateral stability of the vehicle within its stability envelope. The attitude of the vehicle is given by the roll and pitch angle outputs.

incorporate enough sensing and computation to become aware of stability margin and perhaps they will become active in their approaches to the management of it.

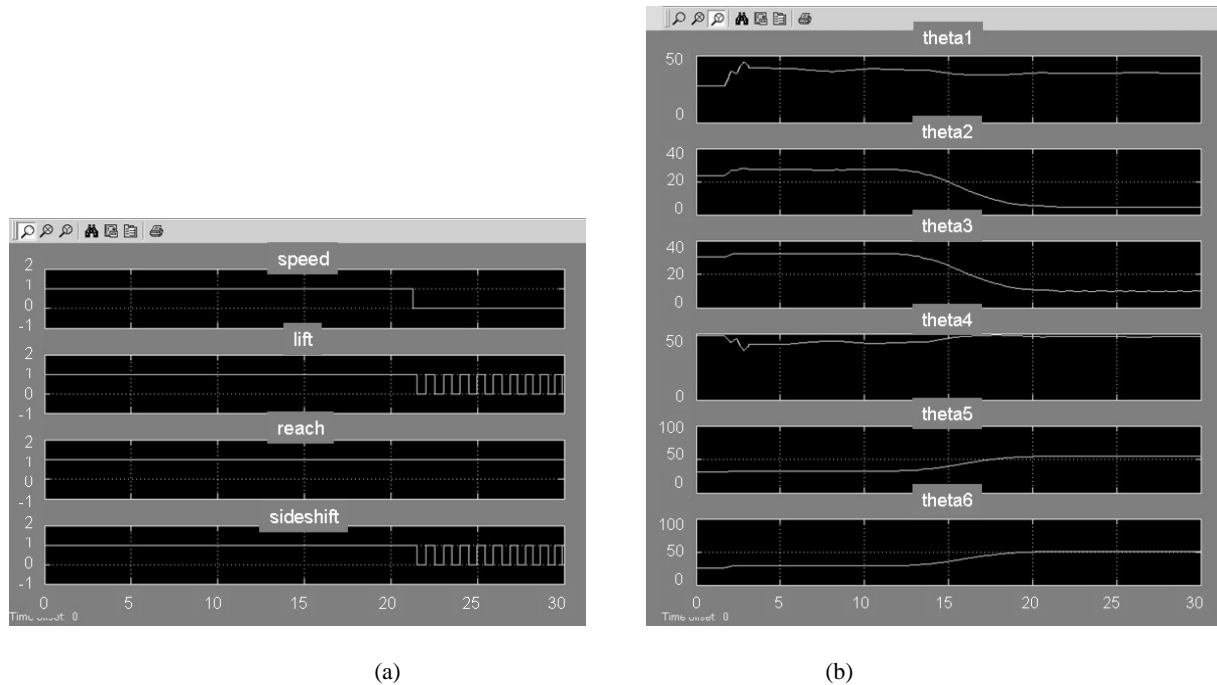


Fig. 13. Case A: (a) Computed governing actions. (b) Stability margin expressed as the angle of the resultant (degrees). This vehicle has six candidate tipover axes hence the six resultant angles. Resultant angles associated with the tipover axes 2 and 3 decrease since these axes are the candidate tipover axes for this maneuver. Axes 5 and 6 are on the opposite side therefore their associated angles increase. Finally, axes 1 and 4 correspond to the front and rear tipover axes (e.g., longitudinal tipover).

Acknowledgment

The work described in this paper was done while both authors were employed by The Robotics Institute, Carnegie Mellon University. Dr. Antonio Diaz-Calderon is currently employed by Jet Propulsion Laboratory, California Institute of Technology through a contract with the National Aeronautics and Space Administration. The work described in this paper is not associated with JPL, Caltech or NASA.

References

1. Barshan, B. and H. F. Durrant-Whyte: 1995, 'Inertial navigation systems for mobile robots'. *IEEE Transactions on Robotics and Automation* **11**(3), 328–342.
2. Blakenship, J. W., K. H. Means, and C. J. Biller: 1984, *Side slopes static stability of double articulated logging tractors*. Society of Automotive Engineers Technical Paper No. 841140.

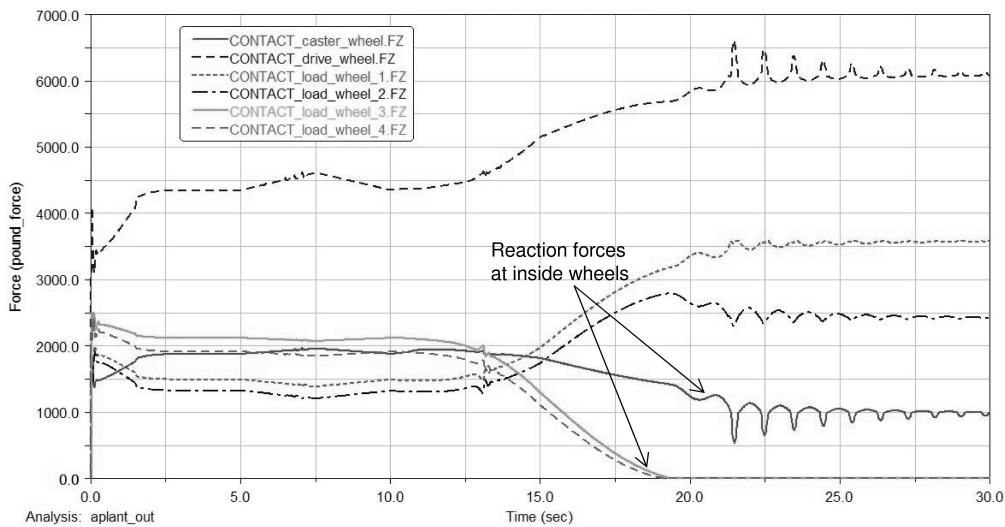


Fig. 14. Case A: Wheel reaction forces. Wheel reaction forces for the inside wheels approach zero as the vehicle reaches marginal stability.

3. Buchele, W. and L. Xie: 1990, 'Computer analysis of the lateral stability of agricultural tractors'. In: *American Society of Agricultural Eng. Winter Meeting*.
4. Chrstos, J. P. and D. A. Guenther, *The measurement of static rollover metrics*. Society of Automotive Engineers Technical Paper No. 920582.
5. Conte, S. D. and C. W. De Boor: 1980, *Elementary numerical analysis: An algorithmic approach*, International series in pure and applied mathematics. McGraw-Hill Higher Education, 3rd edition.
6. Davidson, J. K. and G. Schweitzer: 1990, 'A mechanics based computer algorithm for displaying the margin of static stability in four legged vehicles'. *Trans ASME J. Mechanical Design* **112**, 480–487.
7. Dubowsky, A. and E. E. Vance: 1989, 'Planning mobile manipulator motions considering vehicle dynamic stability constraints'. In: *IEEE International Conference on Robotics and Automation*, Vol. 3. pp. 1271–1276.
8. Dugoff, H., P. Fancher, and L. Segel: 1970, *An analysis of tire traction properties and their influence on vehicle dynamic performance*. Society of Automotive Engineers Technical Paper No. 7000377.
9. Fukuda, T., Y. Fujisawa, K. Kosuge, F. Arai, E. Muro, H. Hoshino, T. Miyazaki, K. Utubo, and K. Uehara: 1992, 'Manipulator/vehicle system for man-robot cooperation'. In: *IEEE Intlernational Confonference on Robotics and Automation*, Vol. 1. pp. 74–79.
10. Genta, G.: 1999, *Motor vehicle dynamics: Modeling and simulation*, Vol. 43 of *Series on Advances in Mathematics for Applied Sciences*. Singapore: World Scientific.
11. Ghasempoor, A. and N. Sepehri: 1995, 'A measure of machine stability of moving base manipulators'. In: *IEEE International Conference on Robotics and Automation*, Vol. 3. Nagoya, Japan, pp. 2249–2254.
12. Gillespie, T. D.: 1992, *Fundamentals of vehicle dynamics*. Warrendale, PA: Society of Automotive Engineers.

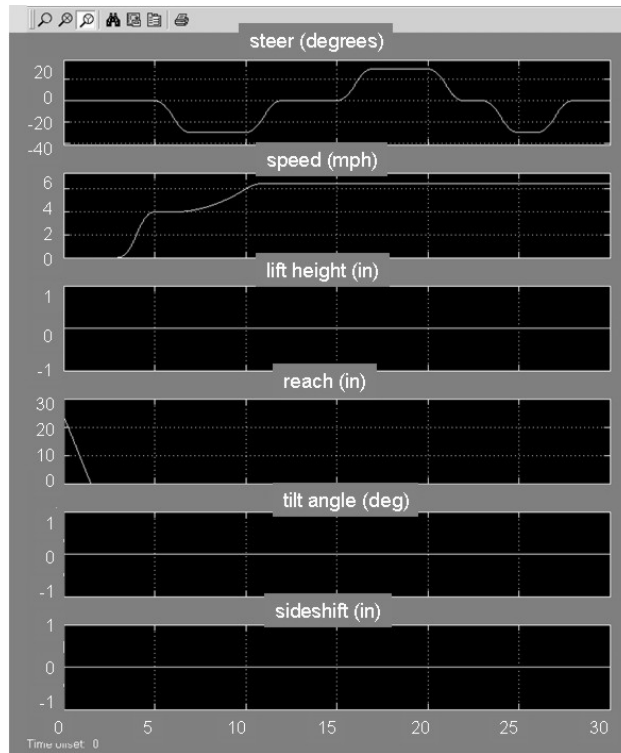
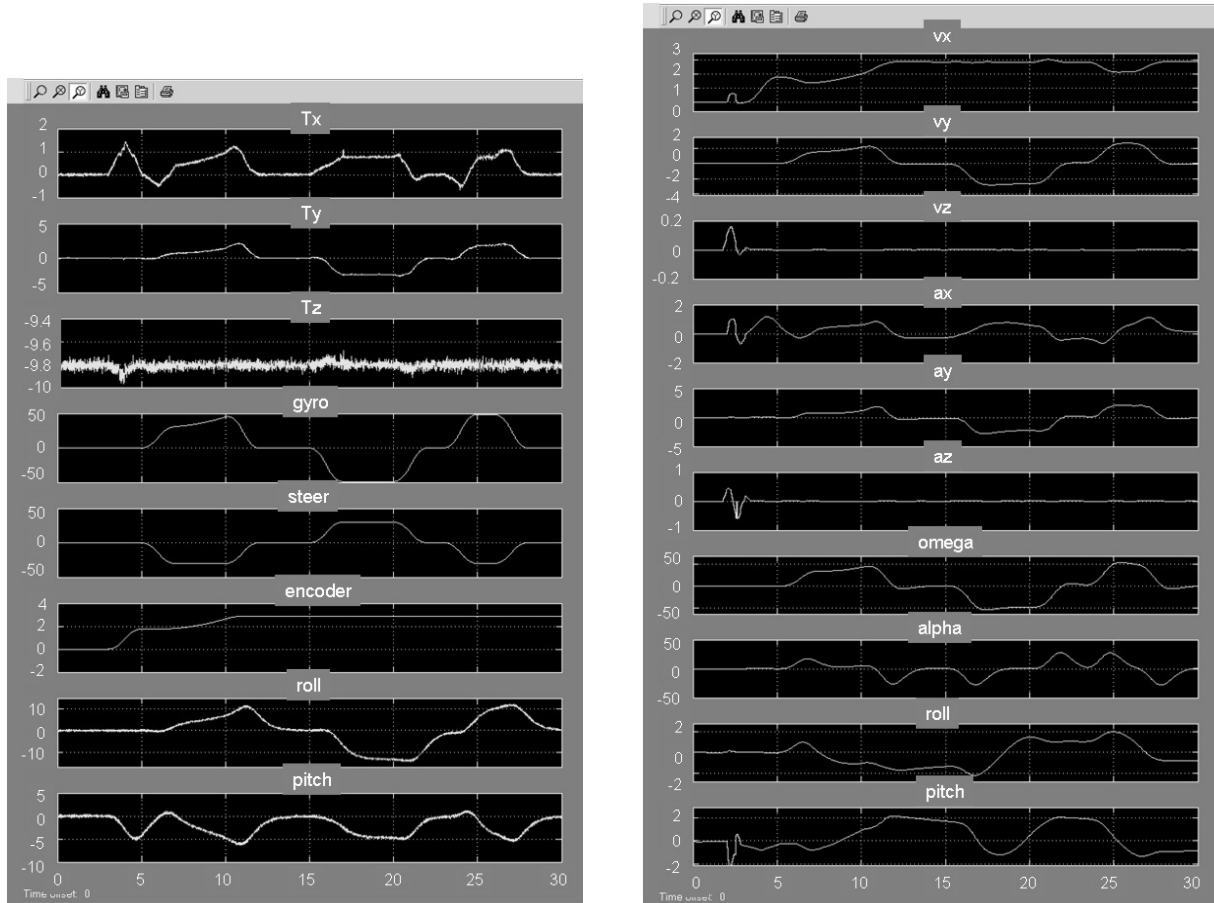


Fig. 16. Case B: Drive inputs.

24. McGhee, R. B. and G. I. Iswandhi: 1979, 'Adaptive locomotion of a multilegged robot over rough terrain'. *IEEE Transactions on Systems, Man and Cybernetics* **SMC-9**(4), 176–182.
25. McGhee, R. B., F. Ozguner, and S. J. Tsai: 1984, 'Rough terrain locomotion by a hexapod robot using a binocular ranging system'. In: M. Brady and R. Paul (eds.): *Robotics Research*. Cambridge, MA: MIT Press, pp. 227–251.
26. Messuri, D. A. and C. A. Klein: 1985, 'Automatic body regulation for maintaining stability of a legged vehicle during terrain locomotion'. *IEEE Journal of Robotics and Automation* **1**(3), 132–141.
27. MSC: 2003, 'MSC.ADAMS'. <http://www.mscsoftware.com>.
28. Muybridge, E.: 1957, *Animals in Motion*. New York: Dover.
29. Papadopoulos, E. G. and D. A. Rey: 1996, 'A new measure of tipover stability margin for mobile manipulators'. In: *IEEE International Conference on Robotics and Automation*.
30. Papadopoulos, E. G. and D. A. Rey: 2000, 'The force-angle measure of tipover stability margin for mobile manipulators'. *Vehicle System Dynamics* **33**, 29–48.
31. Raibert, M. H.: 1983, 'Dynamic stability and resonance in a one-legged hopping machine'. In: A. Morecki, G. Bianchi, and K. Kedzior (eds.): *Proceedings of RoManSy '81*. Warsaw, pp. 352–367.
32. Rey, D. A. and E. G. Papadopoulos: 1997, 'On-line automatic tipover prevention for mobile manipulators'. In: *IEEE/RSJ Int. Conf. on Intelligent Robots and Systems (IROS)*.



(a)

(b)

Fig. 17. Case B: (a) Simulated sensor indications. (b) Vehicle cg state.

33. Roumeliotis, S. I., A. E. Johnson, and J. F. Montgomery: 2002, 'Augmenting inertial navigation with image-based motion estimation'. In: *IEEE International Conference on Robotics and Automation*. pp. 4326–4333.
34. Rudolph, A.: 2003, 'Quantification and estimation of differential odometry errors in mobile robotics with redundant sensor information'. *International Journal of Robotics Research* **22**(2).
35. Schramm, H., F. Hecker, O. Jundt, K. Dieter, and I. Faye: 1997, 'Vehicle dynamics control for commercial vehicles'. In: *International Truck & Bus Meeting & Exposition*. Cleveland, OH. Society of Automotive Engineers Technical Paper No. 973284.
36. Shen, C. N. and C. S. Kim: 1980, 'A laser rangefinder path selection system for martian rover using logarithmic scanning scheme'. In: C. W. Munday (ed.): *Automatic Control in Space. Proceedings of the 8th IFAC Symposium*. Oxford, UK: Pergamon Press, pp.

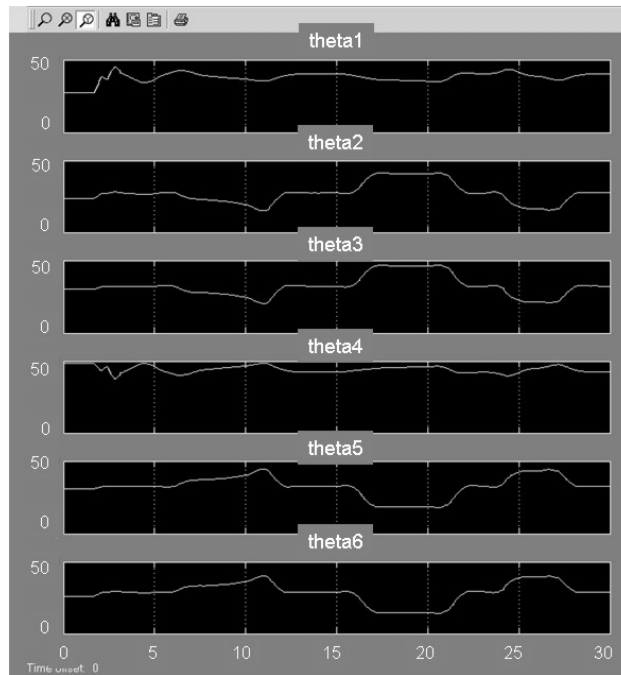


Fig. 18. Case B: Stability margin expressed as the angle of the resultant (degrees) for the variable curvature/variable speed experiment.

- 323–330.
37. Shiller, Z. and Y. R. Gwo: 1991, 'Dynamic motion planning of autonomous vehicles'. *IEEE Transactions on Robotics and Automation* **7**(2), 241–249.
 38. Song, S. M. and K. Waldron: 1989, *Machines that Walk*. Cambridge, MA: MIT Press.
 39. Sreenivasan, S. V. and B. H. Wilcox: 1994, 'Stability and traction control of an actively actuated micro-rover'. *Journal of Robotics Systems* **11**(6).
 40. Steiner, P., P. Weidel, H. Kublbeck, H. Steurer, P. Hora, and D. Zechmair, *Rollover detection*. Society of Automotive Engineers Technical Paper No. 970606.
 41. Sugano, S., Q. Huang, and I. Kato: 1993, 'Stability criteria in controlling mobile robotic systems'. In: *IEEE/RSJ International Conference on Intelligent Robots and Systems '93, IROS '93*. Yokohama, Japan, pp. 832–838.
 42. Sukkariéh, S., E. M. Nebot, and H. F. Durrant-Whyte: 1999, 'A high integrity IMU/GPS navigation loop for autonomous land vehicle applications'. *IEEE Transactions on Robotics and Automation* **15**(3), 572–578.
 43. UMTRI: 1991, 'Mechanics of heavy duty trucks and truck combinations'. Technical Report UMTRI-80868, Transportation Research Institute, The University of Michigan. Engineering Summer Conferences.
 44. Vukobratovic, M., A. Frank, and D. Juricic: 1970, 'On the Stability of Biped Locomotion'. *IEEE Trans Biomedical Engineering* **BME-17**(1).

45. Wallner, E. and J. K. Schiffmann: 2000, 'Development of an Automotive Rollover Sensor'. In: *SAE 2000 Automotive Dynamics & Stability Conference*. Detroit, MI. Society of Automotive Engineers Technical Paper No. 2000-01-1651.
46. Wettergreen, D. and C. Thorpe: 1992, 'Gait generation for legged robots'. In: *IEEE/RSJ international Conference on Intelligent Robots and Systems*, Vol. 2. pp. 1413–1420.
47. Winkler, C. B., D. Blower, R. D. Ervin, and R. M. Chalasani: 2000, *Rollover of heavy commercial vehicles*. Warrendale, PA: Society of Automotive Engineers.